Int. J. Heat Mass Transfer. Vol. 36, No. 4, pp. 845-856, 1993
Printed in Great Britain

0017-9310/93 $6.00+0.00

Effects of stress work on similarity solutions of mixed convection in rotating channels with wall-transpiration

C. Y. SOONG
Department of Aeronautical Engineering, Chung Cheng Institute of Technology, Taoyuan, Taiwan 33509, R.O.C.

and

G. J. HWANG†
Department of Power Mechanical Engineering, National Tsing Hua University, Hsinchu, Taiwan 30043, R.O.C.

(Received 28 May 1992)

Abstract—The effects of stress work on similarity solutions of mixed convection in radially rotating channels with wall-transpiration are dealt with. Imposing proper geometric limitations, constant wall-transpiration, and linear wall-temperature distribution, similarity equations for two classes of rotating channel flows are developed: (1) effects of viscous dissipation and compression work on mixed convection in a rotating solid-walled channel, and (2) the effect of compression work on mixed convection in a rotating semiporous-walled channel with transpiration. Flow and heat transfer characteristics with the effects of the centrifugal-buoyancy, Coriolis force, wall-transpiration, viscous dissipation and compression work are discussed in the similarity solutions. The present study gives a better understanding of the complex mixed convection problem.

INTRODUCTION

ROTATING channel flow and heat transfer are closely related to convective heat transfer in thermal systems such as gas turbines and rotating electrical machinery. It is also attractive academically due to the complexity in flow structure under the influence of rotation. In the literature the effects of Coriolis-induced secondary flow and centrifugal-buoyancy on convective heat transfer have been studied extensively, e.g. theoretical analyses [1, 2], numerical studies [3, 4] and experimental investigations [5–9]. Furthermore, if the wall-transpiration effect is considered, more complexities could be introduced, and only a few two-dimensional studies are available for this type of flow. Since the typical transpiration cooling channels are of low cross-sectional aspect-ratios [10, 11], a two-dimensional analysis is proper for understanding of the convection mechanism. Epifanov *et al.* [12] carried out an integral analysis to determine the forced convection heat transfer rate. Soong and Hwang [13] performed a theoretical analysis on mixed convection and flow-reversal in rotating semiporous-walled channels without stress work.

In a rotating thermal system, high rotation rate may induce significant Coriolis and centrifugal-buoyancy forces, and stress works including viscous dissipation and compression work. The stress works have been considered in natural convection [14–16] and mixed convection [17–19] in gravitational force field. In a rotating disk system, Chew [20] has also advocated the significance of the stress works. To the authors' best knowledge, mixed convection with stress work effects in radially rotating channels has not been reported yet.

By considering the effects of stress works, the previous analysis [13] is further extended in the present study. A theoretical model is proposed for studying the rotation-induced buoyancy, wall-transpiration and especially, the stress work effects. Assuming a large semi-span eccentricity and slenderness of the channel, and imposing the thermal boundary condition of a constant wall-temperature gradient, similarity equations for two classes of flow configurations are rigorously developed. They are: (1) mixed convection with both compression work and viscous dissipation in a radially rotating solid-walled channel; and (2) mixed convection with compression work effect in a one-sided porous-walled channel. The similarity equations are solved and the effects of rotation, transpiration, and stress works on the hydrodynamic and thermal characteristics are examined. A closed-form analytical solution can be found readily for some solid-walled channel flows. Flow-reversal can be induced by wall-transpiration and buoyancy effects.

†Author to whom all correspondence should be addressed.

NOMENCLATURE

C_f	skin friction coefficient
c_p	constant pressure specific heat
Ec	Eckert number, $U_0^2/c_p\Delta T$
Ec^*	reduced Eckert number, Ec/Re
f	dimensionless stream function or transverse velocity, V/V_w
G_ω	rotational G-number, $(X_e\omega^2)H/c_p\Delta T$
g	dimensionless temperature, $(T-T_{sw})(Pe\,\Delta T_c u_m)$
H	channel height
h	heat transfer coefficient
k	thermal conductivity
L	channel length
Nu	Nusselt number, hH/k
P	pressure
$\bar{P}$	reduced pressure, $P+(\rho\omega^2/2)[(X\pm X_0)^2+Y^2]$
P', p'	dimensional and dimensionless pressure departure, $p' = P'/\rho_r U_0^2$
Pe	Peclet number, $Pr\ Re$
Pr	Prandtl number, ν/α
$\mathbf{R}$	position vector emanating from rotation center
Ra_ω	rotational Rayleigh number, $(X_e\omega^2\beta\Delta T_c H^3\ Pr)/\nu^2$
Re	main flow Reynolds number, U_0H/ν
Re_x	Reynolds number based on local mean velocity, $U_m H/\nu$
Re_w	wall suction Reynolds number, $V_w H/\nu$
Ro	rotation number, $\omega H/U_0$
T	temperature
ΔT_c	characteristic temperature difference
U, V	velocity components
U_0	mean velocity at $X=0$
U_m, u_m	dimensional and dimensionless local mean velocity, $U_m(X) = U_0 u_m$
u, v	dimensionless velocity components, U/U_0 and V/U_0
X, Y	Cartesian coordinates
x, y	dimensionless coordinates, X/H and Y/H
X_e, x_e	dimensional and dimensionless semi-span eccentricity, $X_e = Hx_e$.

Greek symbols

α	thermal diffusivity
β	thermal expansion coefficient
δ	dimensionless wall temperature difference, $(T_{pw}-T_{sw})/(Pe\,\Delta T_c u_m)$
δ^*	wall temperature difference parameter, $\delta/(1-G_\omega)$
θ	dimensionless temperature difference, $(T-T_r)/\Delta T_c$
μ	viscosity
ν	kinematic viscosity
Π	pressure-drop parameter, $\int_0^1[(-Re_x/\rho U_m^2)\times(\partial\bar{P}/\partial x)+2Ro\,Re_w(U_0/U_m)f]\,dy$
ρ	density
τ	solid wall temperature gradient
ϕ	viscous dissipation function
ψ	stream function
ω	rotation speed.

Subscripts

cr	critical condition
m	mean
pw	porous wall
r	reference condition
sw	solid wall
ω	rotation condition.

The effects of stress work on the threshold of the flow-reversal are also studied.

THEORETICAL ANALYSIS

Flow configuration and governing equations

Figure 1 shows a channel consisting of two parallel walls, one solid and the other porous, separated by a spacing H and rotating at a speed ω about an axis perpendicular to the axis of the channel. The axis of rotation lies at a distance X_0 away from the channel entrance. The main stream flows along the channel axis and bleeds out through the porous-wall at a transpiration velocity $V_w(X)$. The main stream may flow radially outward or inward, as shown in Figs. 1(a) and (b), respectively. In the analysis, the flow is assumed to be laminar and steady, and the compression work and viscous dissipation are considered. Since the buoyancy effect becomes significant in the presence of the high centrifugal acceleration, Boussinesq's approximation is invoked to allow for a linear variation of density with temperature in the centrifugal force term. Gravitational effect in this problem is relatively small and can be neglected.

Subject to the above assumptions, the conservations of mass, momentum and energy in vector form are depicted as follows:

$$\nabla\cdot V = 0 \tag{1}$$

$$(V\cdot\nabla)V = \nu\nabla^2V-\nabla P'/\rho+\beta(T-T_r)(\omega\times\omega\times\mathbf{R}) -2\omega\times V \tag{2}$$

$$(V\cdot\nabla)T = \alpha\nabla^2T+V\cdot\nabla P/\rho c_p+\mu\phi/\rho c_p \tag{3}$$

where the subscript r denotes the condition at origin (0, 0) and is used as the reference condition, $P' = P-P_r$ the pressure departure from the reference condition, $\mathbf{R}$ the position vector emanating from the

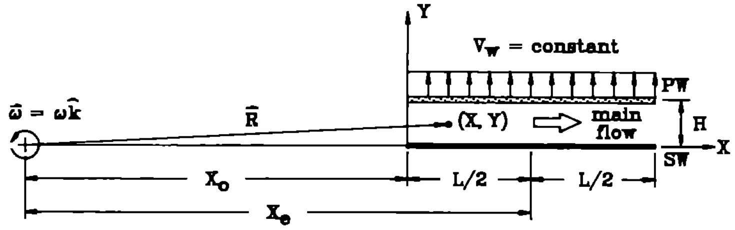

(a) Radially outward flow, $\vec{R} = (X + X_o)\,\hat{i} + Y\,\hat{j}$

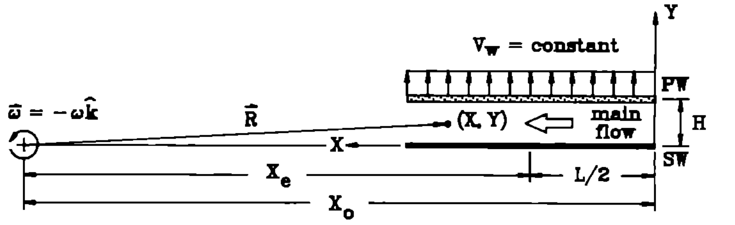

(b) Radially inward flow, $\vec{R} = (X - X_o)\,\hat{i} + Y\,\hat{j}$

FIG. 1. Physical configuration and coordinate system.

rotation center and $\phi = 2[(\partial U/\partial X)^2+(\partial V/\partial Y)^2]+(\partial U/\partial Y+\partial V/\partial X)^2$ the dissipation function. Assuming the channel is very slender and the axial velocity U is much larger than that of the transverse velocity V, only the term $(\partial U/\partial Y)^2$ in ϕ remains. The radial direction hydrostatic pressure distribution is $P_r = P_0+(1/2)\rho(X\pm X_0)^2\omega^2$. The term $V\cdot\nabla P$ means the work done per unit time per unit volume. Furthermore, by substituting the pressure distribution into $V\cdot\nabla P$ one has approximately $U\cdot\rho(X\pm X_0)\omega^2$. This means the work is done by the product of radial velocity and weight of air per unit volume. It is noted that the weight of air may become extremely large due to the high speed rotation. Therefore, the compression work term can be written as

$$V\cdot\nabla P/\rho c_p \approx (1/\rho c_p)U\partial P_r/\partial X = \omega^2(X\pm X_0)U/c_p.$$

Finally, the governing equations can be written in dimensionless forms as

$$\frac{\partial u}{\partial x}+\frac{\partial v}{\partial y} = 0 \tag{4}$$

$$u\frac{\partial u}{\partial x}+v\frac{\partial u}{\partial y} = \frac{1}{Re}\nabla^2 u-\frac{\partial p'}{\partial x} - \frac{Ra_\omega}{Pe\,Re}\left(\frac{x\pm x_0}{x_e}\right)\theta+2Ro\,v \tag{5}$$

$$u\frac{\partial v}{\partial x}+v\frac{\partial v}{\partial y} = \frac{1}{Re}\nabla^2 v-\frac{\partial p'}{\partial y} - \frac{Ra_\omega}{Pe\,Re}\left(\frac{y}{x_e}\right)\theta-2Ro\,u \tag{6}$$

$$u\frac{\partial \theta}{\partial x}+v\frac{\partial \theta}{\partial y} = \frac{1}{Pe}\nabla^2\theta+G_\omega\frac{x\pm x_0}{x_e}u+Ec^*\left[\frac{\partial u}{\partial y}\right]^2; \tag{7}$$

by using the transformations

$$u = U/U_0,\quad v = V/U_0,\quad x = X/H,\quad y = Y/H,$$
$$p' = P'/\rho_r U_0^2,\quad \theta = (T-T_r)/\Delta T_c,$$
$$Re = U_0 H/\nu,\quad Pe = Pr\,Re,\quad Ro = \omega H/U_0,$$
$$Ra_\omega = (X_c\omega^2\beta\Delta T_c H^3\,Pr)/\nu^2,$$
$$G_\omega = (X_c\omega^2)H/c_p\Delta T_c,\quad Ec = U_0^2/c_p\Delta T_c,$$
$$Ec^* = Ec/Re$$

where U_0 is the mean velocity at $X = 0$, $T_r = T_{sw}(0)$ the solid-wall temperature at $X = 0$ and ΔT_c the characteristic temperature difference to be determined later. The boundary conditions at the solid wall, $y = 0$, are $u = v = \theta-\theta_{sw}(x) = 0$; and at the porous wall, $y = 1$, are $u = v-v_w = \theta-\theta_{pw}(x) = 0$, in which the subscripts sw and pw denote the solid and porous wall, respectively.

Similarity transformation and equations

In this flow configuration, it is expected that the condition of fully-developed flow is not the same as that of the conventional internal flows, that is $\partial u/\partial x = v = \partial\theta/\partial x = 0$. Since the fluid bleeds out through the porous wall at a rate of $\rho V_w(X)$ per unit area, the mass balance along the channel length is

$$\rho U_m(X)Hb = \rho U_0 Hb - b\int_0^X \rho V_w(x)\,\mathrm{d}X,$$

where h is the channel depth, or in a dimensionless form:

$$u_m(x) = 1 - \int_0^x v_w(x)\,dx \quad (8)$$

for a constant density ρ. The mean velocity $u_m(x)$ will be used as a basis for the fully developed invariant profile of axial velocity. To develop the similarity equations, the stream function is expressed in a form of separation of variables, namely

$$\psi(x, y) = u_m(x) f(y) \quad (9)$$

where $f(y)$ is an invariant in x-direction and it may exist under a certain form of transpiration velocity $v_w(x)$. By using $u = \partial\psi/\partial y$ and $v = -\partial\psi/\partial x$, one has

$$u(x, y) = u_m(x) f'(y) \quad \text{and} \quad v(x, y) = -u'_m(x) f(y) \quad (10)$$

where $'$ denotes the differentiation. Combining equations (5) and (6) one obtains

$$f^{iv} + Re\, u'_m(ff''' - f'f'') + 2\left(\frac{u''_m}{u_m}\right) f'' - Re\left(u'''_m - \frac{u_m u''_m}{u_m}\right) ff' + \frac{u'''_m}{u_m} f = \frac{Ra_\omega}{Pe \cdot u_m}\left[\frac{x \pm x_0}{x_c}\theta_y - \frac{y}{x_c}\theta_x\right]. \quad (11)$$

It is obvious that, to attain a similarity form of equation (11), the least demand for the temperature function is $\theta(x, y) = fn(x) + \text{const} \cdot u_m(x) \cdot g(y)$, where $fn(x)$ is a certain function of x. For convenience, define

$$\theta(x, y) = \theta_{sw}(x) + Pe\, u_m(x) g(y) \quad (12)$$

where $\theta_{sw}(x)$ is a prescribed solid-wall temperature distribution, and $g(y)$ the x-invariant temperature function. With the aid of equation (12) momentum equation (11) and energy equation (7) become

$$f^{iv} + Re\, u'_m(ff''' - f'f'') + 2\left(\frac{u''_m}{u_m}\right) f'' - Re\left(u'''_m - \frac{u'_m u''_m}{u_m}\right) ff' + \frac{u'''_m}{u_m} f = Ra_\omega\left[\frac{x \pm x_0}{x_c} g' - \frac{y}{x_c}\left(\frac{\theta'_{sw}}{Pe\, u_m} + \frac{u'_m}{u_m} g\right)\right]; \quad (13)$$

$$g'' + Pe\, u'_m(fg' - f'g) + \frac{u''_m}{u_m} g = \left(\theta'_{sw} - G_\omega \frac{x \pm x_0}{x_c}\right) f' - Ec^* u_m (f'')^2 - \frac{\theta''_{sw}}{Pe\, u_m}. \quad (14)$$

The two functions $v_w(x)$ and $\theta_{sw}(x)$ are to be determined by satisfying certain restrictions. For simplicity, the following assumptions are employed:

(1) The wall-transpiration velocity is constant, that is, $u'_m(x) = -v_w = \text{constant}$ and $u''_m = u'''_m = 0$.

(2) Ratios of channel length to semispan eccentricity and channel height to length are sufficiently small, that is L/X_c and $H/L \ll 1$. Consider, for example, a turbine disk of radius 350 mm, and turbine blades of span 80 mm, the hydraulic diameter of cooling channel is of order of 1 mm. Then, referring to Fig. 1, one has the approximations: $(x \pm x_0)/x_c \approx \pm 1$, $y/x_c \ll 1$ and $\theta_y \gg \theta_x$. Thus, the r.h.s. of equation (13) reduces to $\pm Ra_\omega \cdot g'$, and the parenthesis on the r.h.s. of (14) reduces to $(\theta'_{sw} - G_\omega)$.

(3) The viscous dissipation term in equation (14), $Ec^* u_m(x)(f'')^2$, can be x-independent only if u_m is a constant, that is, in the case of solid-walled channel or zero-transpiration ($u_m = 1$). Otherwise, this term must be neglected by assuming the small viscous dissipation effect.

(4) The solid-wall temperature-gradient is constant, that is, $\theta'_{sw}(x) = \text{constant}$. Therefore, without loss of generality, specify $\theta'_{sw} = 1$ or $T_{sw}(x) = T_{sw}(0) + \Delta T_c x$. The characteristic temperature difference can now be determined as $\Delta T_c = \tau_{sw} H$, in which τ_{sw} is a prescribed solid-wall temperature gradient. The function $g(y)$ becomes

$$g(y) = \frac{T(x, y) - T_{sw}(x)}{Pe\, u_m \tau_{sw} H}.$$

At the porous wall, $y = 1$, wall temperature can be specified as $g(1) = [T_{pw}(x) - T_{sw}(x)]/[Pe\, u_m \tau_{sw} H] = \delta$ or, in other words, $T_{pw}(x) = T_{sw}(x) + \delta\, Pe\, u_m \tau_{sw} H$. If $T_{sw}(x)$ and $u_m(x)$ are both linear in x, the porous-wall temperature $T_{pw}(x)$ is also a linear one. The parameter δ represents the temperature difference between the solid and the porous walls and, therefore, it is also an index of asymmetric wall heating.

As listed in Table 1 four possible cases for the present configuration can be classified into two categories, the buoyancy-opposed mixed convection with $Ra_\omega(x \pm x_0)/x_c > 0$ and buoyancy-assisted one with $Ra_\omega(x \pm x_0)/x_c < 0$. To unify the equation of motion, the sign of $(x \pm x_0)/x_c$ ($\approx \pm 1$) can be absorbed into the parameter Ra_ω. The positive Ra_ω is responsible for the case of buoyancy-opposed flow and the negative Ra_ω stands for the case of buoyancy-assisted flow.

With assumptions (1)–(4), two sets of similarity equations can be attained from equations (13) and (14):

Class 1: mixed convection with stress work effects in a rotating solid-walled channel, that is, $Re_w = 0$ (or $u_m = 1$), $G_\omega \geqslant 0$, and $Ec^* \geqslant 0$

$$f^{iv} = Ra_\omega g' \quad (15)$$

$$g'' = (1 - G_\omega) f' - Ec^*(f'')^2. \quad (16)$$

Class 2: mixed convection with effects of transpiration and compression work

$$f^{iv} - Re_w(ff''' - f'f'') = Ra_\omega g' \quad (17)$$

Table 1. Possible situations of the present flow configuration

Main flow	Solid wall	$(x \pm x_0)/x_e$	τ	$Ra_\omega\,(x \pm x_0)/x_e$	Type of mixed convection
outward	hot	$\cong +1$	>0	>0	opposed
outward	cold	$\cong +1$	<0	<0	assisted
inward	hot	$\cong -1$	>0	<0	assisted
inward	cold	$\cong -1$	<0	>0	opposed

$$g'' - Pr\,Re_w\,(fg' - f'g) = (1 - G_\omega)f' \qquad (18)$$

where $Re_w = V_w H/\nu$ is wall-suction Reynolds number. The boundary conditions for both of the classes 1 and 2 are:

$$f(0) = f'(0) = f(1) - 1 = f'(0) = 0$$

$$g(0) = g(1) - \delta = 0. \qquad (19)$$

Flow and heat transfer parameters

Following the conventional definition

$$C_f = 2\mu(\partial U/\partial Y)_w/\rho U_m^2(X) \qquad (20)$$

the skin friction coefficients for solid and porous walls can be expressed respectively as

$$C_{f,sw}\,Re_x = 2f''(0) \quad \text{and} \quad C_{f,pw}\,Re_x = -2f''(1) \qquad (21)$$

where Re_x is the Reynolds number based on the local mean velocity, $U_m H/\nu$.

By using a reduced pressure $\tilde{P} = P + (\rho\omega^2/2) \times [(X \pm X_0)^2 + Y^2]$ and the X-momentum equation, the pressure-drop can be characterized by a cross-sectional average of a combined pressure drop involving the Coriolis effect [11, 19]

$$\Pi = \int_0^1 \left[-\frac{Re_x}{\rho U_m^2}\left(\frac{\partial \tilde{P}}{\partial x}\right) + 2Ro\,Re_w\left(\frac{U_0}{U_m}\right)f \right] \mathrm{d}y$$

$$= -f'''(0) - Ra_\omega \int_0^1 g(y)\,\mathrm{d}y. \qquad (22)$$

The heat transfer rate is characterized by the Nusselt number

$$Nu = hH/k = -(\partial T/\partial Y)_w H/(T_w - T_b) \qquad (23)$$

where

$$T_b(X) = \frac{1}{U_m H}\int_0^H UT\,\mathrm{d}Y$$

is the fluid bulk temperature. The resultant Nusselt numbers at solid and porous walls can be written as

$$Nu_{sw} = g'(0) \bigg/ \int_0^1 f'g\,\mathrm{d}y \qquad (24a)$$

and

$$Nu_{pw} = g'(1) \bigg/ \left(\delta - \int_0^1 f'g\,\mathrm{d}y\right). \qquad (24b)$$

In the case of $Re_w \neq 0$, that is, the solutions of class (2), the integral in equation (24) can be evaluated readily from energy equation (18):

$$\int_0^1 f'g\,\mathrm{d}y = \frac{\delta}{2} + \frac{1}{2Pr\,Re_w}[1 - G_\omega + g'(0) - g'(1)]. \qquad (25)$$

When transpiration is absent, this integral can be evaluated simply by using the analytic solutions of class 1 for zero-transpiration.

Governing parameters

Six non-dimensional groups, Pr, Re_w, Ro, Ra_ω, G_ω and Ec^* are shown in equations (15)–(18) and (22). Pr is the Prandtl number, and Re_w the wall-transpiration Reynolds number. The rotation number Ro and the rotational Rayleigh number Ra_ω characterize the Coriolis force and the centrifugal-buoyancy effects, respectively. It is noted that, for the present configuration, the Coriolis force can only provide a modification of the hydrostatic pressure field through the parameter Ro in equations (22). Stress work parameters the rotational G-number $G_\omega = (X_e\omega^2)H/c_p\Delta T_c$ and the reduced Eckert number $Ec^* = Ec/Re = Re\cdot(\nu/H)^2/c_p\Delta T_c$ indicate the measure of the compression work and viscous dissipation, respectively.

In the laminar flow regime the Reynolds number is of order of 10^3, and the channel height is of order of 1 mm. The spanwise variation of the turbine blade temperature is usually of order of 10^2 K [21]. Assume that the channel length is of order of 10^2 mm, therefore, the characteristic temperature-difference in the present analysis is $\Delta T_c = \tau_{sw}H \sim O(1\ \text{K})$, the rotational speed ω is 10 000 r.p.m., and the fluid properties are evaluated at the temperature 500 K ($\approx$ 1000 F) as the coolant air temperature mentioned in a previous paper [11]. Therefore, magnitudes of the parameters are, $Pr = 0.699 \simeq 0.7$, $Ro \sim 0.028$, $Ec^* \sim 1.40 \times 10^{-3}$, $G_\omega \sim 0.415$ and $Ra_\omega \sim 415$. The transpiration velocity V_w is assumed as $V_w \leqslant 10^{-3}\,U_0$ and, therefore, $Re_w \sim 10$.

In the present study the ranges of the parameters, based on the above discussion, are

$$Pr = 0.7,\quad Re_w \sim O(1)\text{–}O(10),$$
$$Ro \sim O(10^{-2}),\quad Ra_\omega \sim O(10^2)\text{–}O(10^3),$$
$$G_\omega \sim O(10^{-1}),\quad Ec^* \sim O(10^{-3}). \qquad (26)$$

NUMERICAL PROCEDURE

In the present study, a standard fourth-order Runge–Kutta scheme with Newton's correction technique is employed. The step-size is 0.01 in the course of computations. More refined step-size of 0.005 is used for determination of flow-reversal locations. As the wall transpiration Reynolds number Re_w increases the problem becomes very stiff. The numerical procedure converges very slowly and, in some extreme cases, the procedure may even diverge. To improve the convergence characteristics, Aitkin acceleration technique and relaxation factor are used for iteration, and a second-order continuation is applied for the continuous computations with increasing Reynolds number Re_w.

RESULTS AND DISCUSSION

Analytic solutions with $Re_\omega = Ec^* = 0$

Equations for both classes 1 and 2 contain nonlinear terms. In general, they can be solved by the numerical methods, for example a typical shooting method described in the previous work [13]. However, an analytic solution is possible in some circumstances of class 1. Combining equations (15) and (16) one has

$$f^{\mathrm{v}} - Ra_\omega(1-G_\omega)f' = -Ec^*\,Ra_\omega(f'')^2. \qquad (27)$$

The corresponding five boundary conditions are

$$f(0) = f'(0) = f(1)-1 = f'(1) = 0$$

and

$$f'''(0) = Ra_\omega\left[\delta-(1-G_\omega)\int_0^1 f\,\mathrm{d}y - Ec^*\int_0^1\int_0^y (f'')^2\,\mathrm{d}y\,\mathrm{d}y\right]. \qquad (28)$$

Due to the presence of the nonlinear viscous dissipation term, $Ec^*\,Ra_\omega(f'')^2$, equation (27) is not tractable analytically. By neglecting the viscous dissipation effect, equation (27) becomes

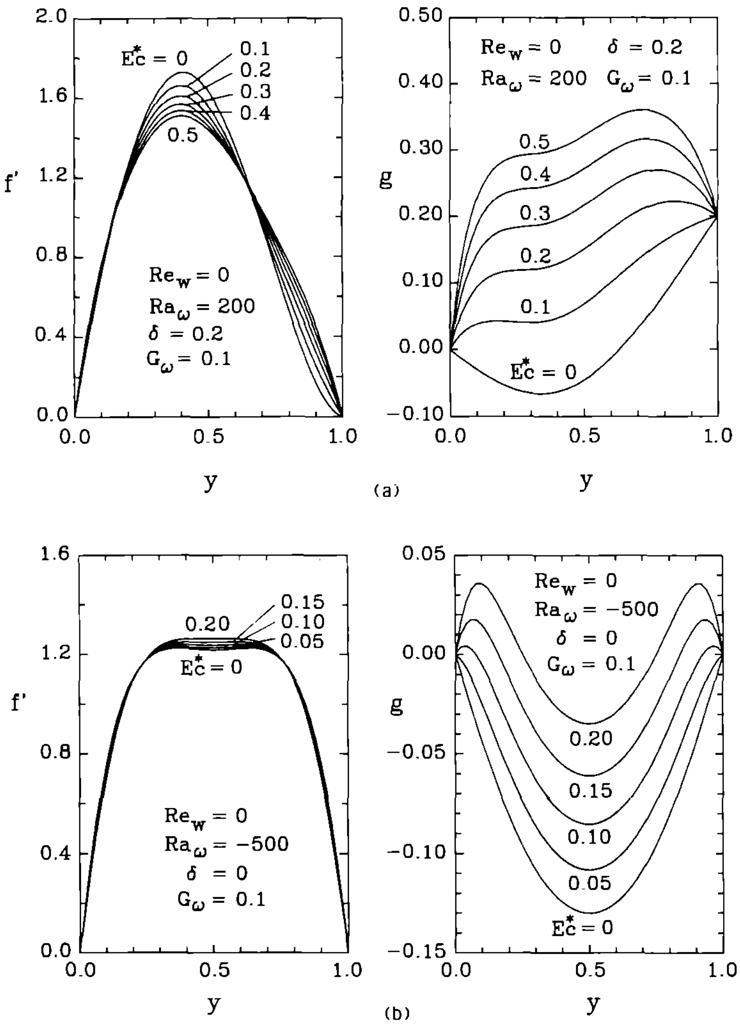

FIG. 2. Viscous dissipation effect in solid-walled channel: (a) buoyancy-opposed flows; (b) buoyancy-assisted flows.

$$f' - Ra_{\omega}(1-G_{\omega})f'' = 0$$

or

$$f''' - Ra_{\omega}(1-G_{\omega})f = f'''(0). \qquad (29)$$

The solutions with $0 \leqslant G_{\omega} < 1$ are different for the cases $Ra_{\omega} = 0$, >0 and <0 corresponding physically to the pure forced convection, buoyancy-opposed and buoyancy-assisted mixed convection, respectively. The analytical solution of equation (29) listed in the Appendix is an extension of the analytical solution in ref. [13] with the consideration of compression work. By setting $G_{\omega} = 0$, the solutions reduce to the closed-form solutions in ref. [13].

Velocity and temperature profiles

To make the viscous dissipation effect clear, the solutions with exaggerated values of Ec^* ($O \sim 10^{-1}$) are calculated. Figure 2(a) shows the viscous dissipation effect on velocity and temperature distributions in outward buoyancy-assisted flows. Due to internal viscous heating, the fluid temperature is raised, the wall-to-fluid temperature difference is decreased, and therefore, the buoyancy effect is suppressed. However, because of the existence of the strong forced flow, the distortion of velocity field is relatively smaller than the change of fluid temperature. This phenomenon is also presented in inward buoyancy-opposed flows in Fig. 2(b). The viscous heating increases the fluid temperature and the velocity near $y = 0.5$. A similar effect for compression work can be observed in Fig. 3(a) for the buoyancy-opposed flows and Fig. 3(b) for the buoyancy-assisted flows.

Figure 4 reveals the compression work effect on the velocity and temperature distributions with wall-transpiration. Figure 4(a) shows a typical buoyancy-opposed flow in which fluid temperature can be heated due to the internal heating caused by the compression

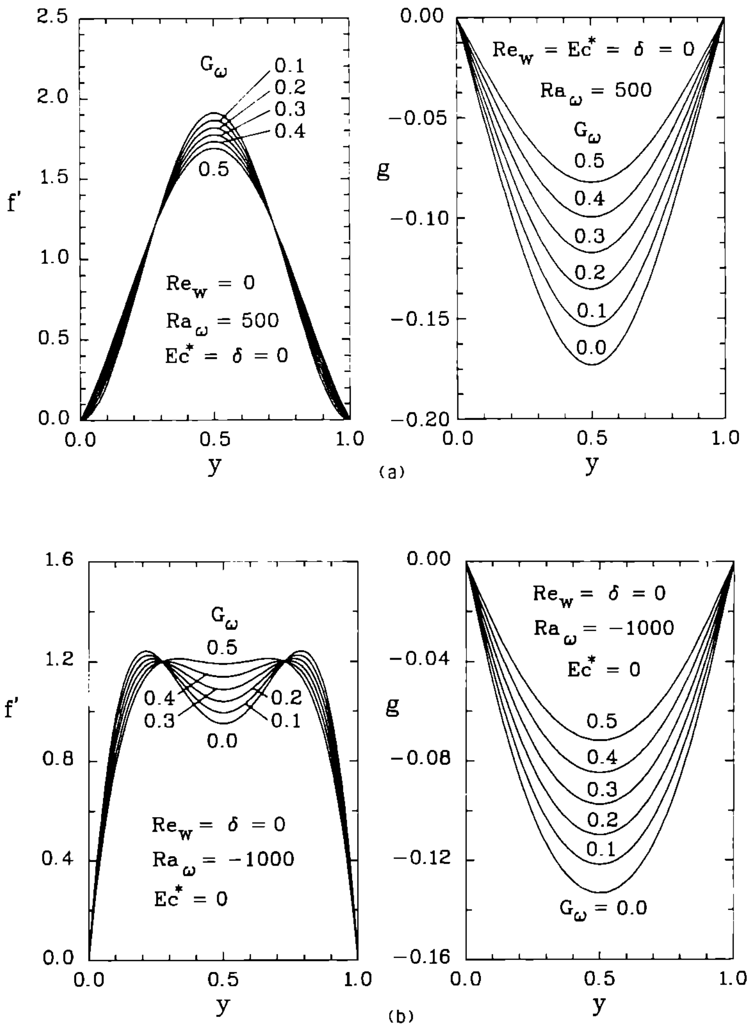

FIG. 3. Compression work effect in solid-walled channel: (a) buoyancy-opposed flows; (b) buoyancy-assisted flows.

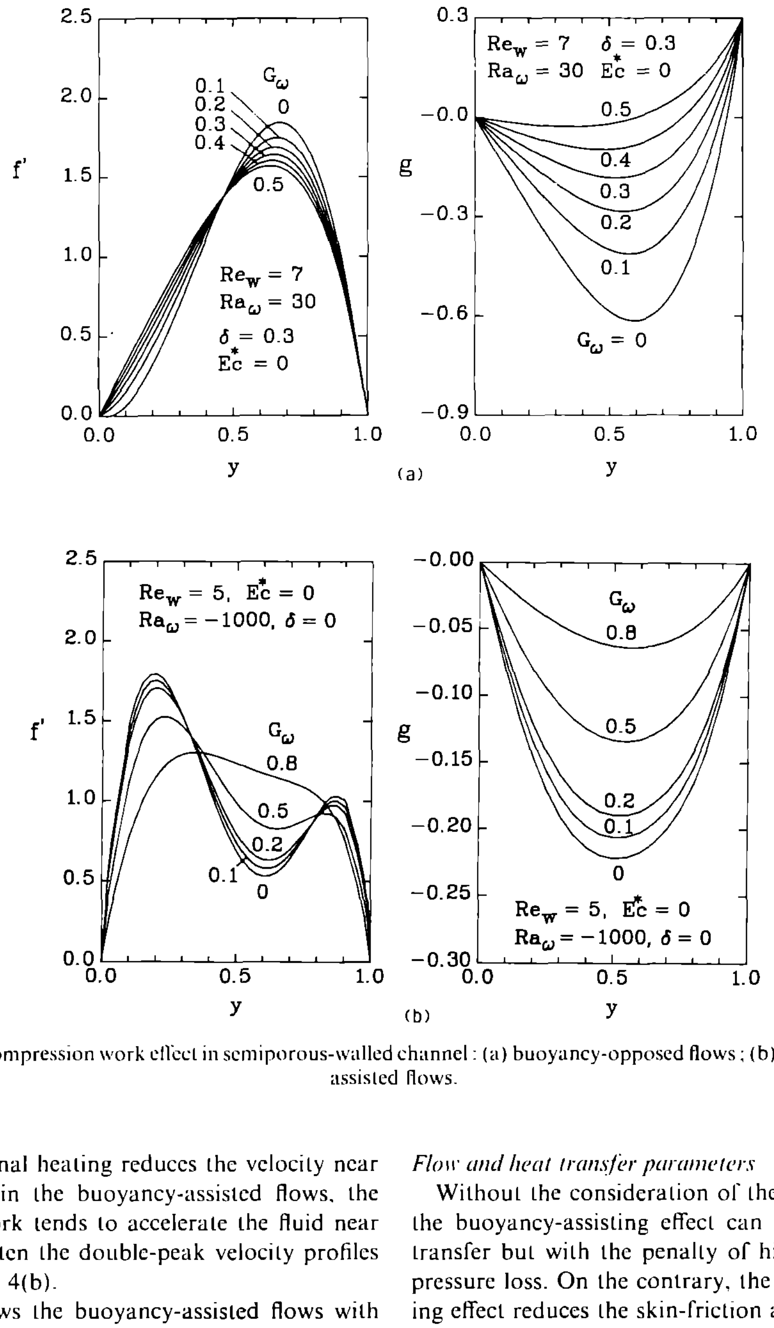

FIG. 4. Compression work effect in semiporous-walled channel: (a) buoyancy-opposed flows; (b) buoyancy-assisted flows.

work. The internal heating reduces the velocity near $y = 0.7$. While in the buoyancy-assisted flows, the compression work tends to accelerate the fluid near $y = 0.5$ and flatten the double-peak velocity profiles as shown in Fig. 4(b).

Figure 5 shows the buoyancy-assisted flows with asymmetric wall-heating and coupled effect of buoyancy and stress work. In this figure, the fluid near the two walls will not be retarded or accelerated in the same manner. The temperature profiles have very high gradients and the velocity profiles have high peaks near the porous wall ($y = 1$). Therefore, there is a stronger buoyancy-assisting effect than that near the solid-wall. If the velocity peak near the porous wall grows further and, due to the global continuity, the velocity peak near the solid wall must be flattened. Most of the main flow moves radially near the porous wall. While the fluid near the solid wall is almost stagnant and the temperature of fluid there tends to be uniform. It can be expected that the heat transfer is poor at the solid wall.

Flow and heat transfer parameters

Without the consideration of the stress work [13], the buoyancy-assisting effect can enhance the heat transfer but with the penalty of higher friction and pressure loss. On the contrary, the buoyancy-opposing effect reduces the skin-friction and pressure-drop as well as the heat transfer rate. To examine the stress work effects on $C_f\ Re_x$, Π, and Nu, results for $Re_w = \delta = 0$ are plotted in Fig. 6. From the discussion in the last section one can easily conclude that the stress effects reduce the temperature gradient $\partial\theta/\partial y$ at walls for both buoyancy-assisted and opposed flows. In buoyancy-assisted flows, the stress work effects decelerate fluid velocity near the walls as shown in Fig. 3(b), and reduce the heat transfer rate. In buoyancy-opposed flows ($Ra_\omega > 0$), the fluid near the walls is accelerated as shown in Fig. 3(a). The resultant heat transfer performance depends on the resultant effect of the two counter factors, that is, reduction of $(\partial\theta/\partial y)_w$ and increase of fluid velocity near the wall region. To provide clear comparisons between the

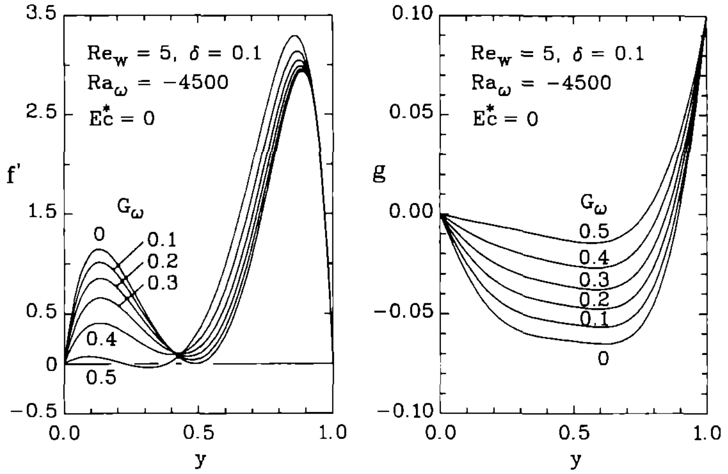

FIG. 5. Compression work effect in semiporous-walled channel with asymmetrical wall-heating.

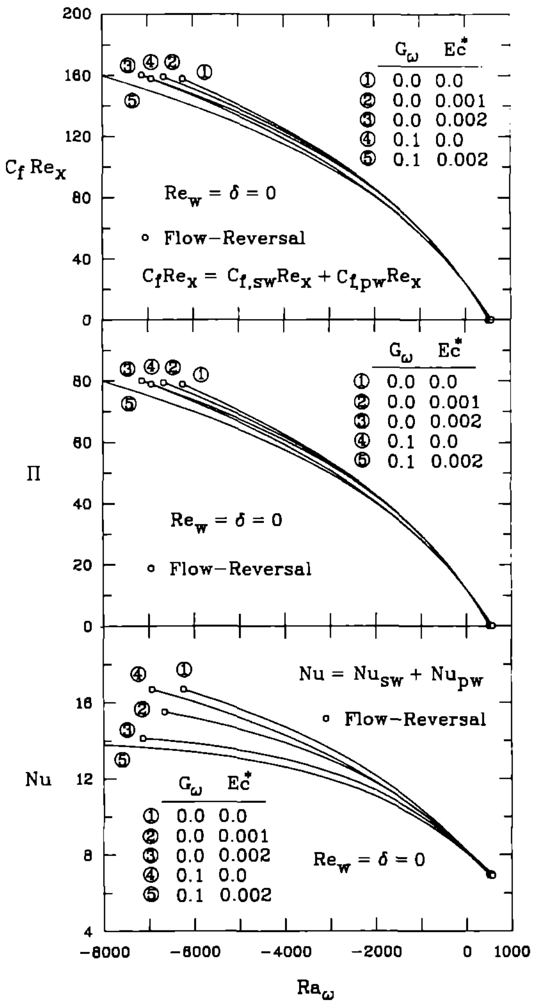

FIG. 6. Flow and heat transfer parameters of mixed convection in radially rotating channel with buoyancy and stress work effects.

data with various stress work effects, Table 2 lists the Nusselt numbers for $Re_w = \delta = 0$. It is observed that for $Ra_\omega > 0$, Nusselt numbers for cases 2 and 3 are smaller than the baseline case 1; while in cases 4 and 5, the values of Nu are larger than those for case 1. However, for the case of $Ra_\omega < 0$, Nusselt numbers are all reduced by the stress work effects. Table 3 shows the stress work effects on the skin friction parameters, the Nusselt numbers and the boundary derivatives $g'(0)$, $g'(1)$, $f''(0)$, and $f''(1)$ for some cases. Due to the definition of Nu shown in equation (23) the stress work effects on the Nusselt numbers seem to be small, however, the values of temperature

Table 2. Stress work effects on Nu for $Re_w = \delta = 0$

	Nu				
Ra_ω	Case 1	Case 2	Case 3	Case 4	Case 5
500	6.9836	6.9666	6.9471	7.1147	7.0669
400	7.2433	7.2198	7.1953	7.3455	7.2870
300	7.4976	7.5682	7.4379	7.5731	7.5023
200	7.7477	7.7115	7.6745	7.7973	7.7125
100	7.9937	7.9497	7.9051	8.0180	7.9176
0	8.2353	8.1827	8.1295	8.2353	8.1176
−500	9.3766	9.2670	9.1567	9.2675	9.0379
−1000	10.4069	10.2200	10.0315	10.2095	9.8299
−2000	12.1615	11.7770	11.3894	11.8405	11.0773
−3000	13.5769	12.9644	12.3488	13.1829	11.9731
−4000	14.7341	13.8828	13.0302	14.2977	12.6162
−5000	15.6983	14.6069	13.5168	15.2370	13.0777
−6000	16.5177	15.1887	13.8639	16.0412	13.4067

Note:

	Ec^*	G_ω
Case 1	0.000	0.0
Case 2	0.001	0.0
Case 3	0.002	0.0
Case 4	0.000	0.1
Case 5	0.002	0.1

Table 3. Stress work effects on flow and heat transfer parameters

	C_{fsw}	C_{fpw}	Nu_{sw}	Nu_{pw}	$f''(0)$	$f''(1)$	$g'(0)$	$g'(1)$
$Re_w = 0$, $Ra_\omega = 500$, $\delta = 0$, $G_\omega = 0$								
Ec^*								
0.000	0.0152	0.0152	3.4925	3.4925	0.0076	−0.0076	−0.5000	0.5000
0.001	0.1683	0.1683	3.4833	3.4833	0.0842	−0.0842	−0.4912	0.4912
0.002	0.3184	0.3184	3.4735	3.4735	0.1592	−0.1592	−0.4824	0.4824
0.003	0.4656	0.4656	3.4633	3.4633	0.2328	−0.2328	−0.4739	0.4739
0.004	0.6100	0.6100	3.4527	3.4527	0.3050	−0.3050	−0.4654	0.4654
0.005	0.7517	0.7517	3.4415	3.4415	0.3758	−0.3758	−0.4570	0.4570
$Re_w = 0$, $Ra_\omega = 500$, $\delta = 0$, $Ec^* = 0$								
G_ω								
0.00	0.0152	0.0152	3.4925	3.4925	0.0076	−0.0076	−0.5000	0.5000
0.10	1.3431	1.3431	3.5573	3.5573	0.6716	−0.6716	−0.4500	0.4500
0.20	2.6390	2.6390	3.6217	3.6217	1.3195	−1.3195	−0.4000	0.4000
0.30	3.9041	3.9041	3.6855	3.6855	1.9520	−1.9520	−0.3500	0.3500
0.40	5.1398	5.1398	3.7488	3.7488	2.5699	−2.5699	−0.3000	0.3000
0.50	6.3473	6.3473	3.8116	3.8116	3.1736	−3.1736	−0.2500	0.2500
$Re_w = 5$, $Ra_\omega = -1000$, $\delta = 0$, $Ec^* = 0$								
G_ω								
0.00	45.5612	41.7405	5.4292	8.0001	22.7806	−20.8702	−0.8444	1.2443
0.10	43.3244	39.6327	5.2773	7.9169	21.6622	−19.8164	−0.7668	1.1503
0.20	40.9107	37.4685	5.1154	7.8350	20.4554	−18.7343	−0.6877	1.0534
0.30	38.2885	35.2555	4.9419	7.7546	19.1443	−17.6277	−0.6073	0.9529
0.40	35.4176	33.0065	4.7547	7.6763	17.7088	−16.5032	−0.5253	0.8481
0.50	32.2460	30.7418	4.5515	7.5998	16.1230	−15.3709	−0.4418	0.7377

gradients $g'(0)$ and $g'(1)$ at walls explain more clearly the heat transfer rates at walls and these can be altered remarkably by the effect of compression work.

Flow-reversal and critical conditions

In the present radially rotating channels, the flow-reversal can be induced by the centrifugal-buoyancy and wall-transpiration. Since the buoyancy effect depends strongly upon the temperature field, the wall-heating (δ) and the stress work (Ec^*, G_ω) effects are also the influential factors for the threshold of flow-reversal. Two modes, wall-flow-reversal (WFR) and in-field flow-reversal (IFR), are presented. The former reveals a one-peak velocity distribution as that shown in Fig. 4(a) and the latter possesses a double-peak velocity profile as shown in Figs. 4(b) and 5. The general feature of the critical conditions for the two modes has been discussed in ref. [13].

Figure 7 shows the stress work effects on the flow-reversal condition for class 1. Due to the internal heating caused by the stress work, the flow-reversal usually can be postponed and the flow-reversal-free (FRF) region in the critical parameter map is enlarged. The effects are not noticeable in the cases with low Rayleigh number. From equations (28), it is very clear that the viscous dissipation effect can alter the flow field through the nonlinear term $-Ec^*(f'')^2$. Since Ec^* is typically of order of 10^{-3}, this effect can be pronounced only at large values of Ra_ω. As for the compression work effect, cases with $G_\omega = 0.1$ were considered. The corresponding term is $Ra_\omega(1-G_\omega)f'$ in equation (28) or (30). It is found that the effect is significant also at large Ra_ω.

In the presence of wall-transpiration the flow-reversal mechanism becomes coupled and complicated. The symmetry of the parameter map displayed in Fig. 7 is destroyed. The compression work effect on the critical condition of flow-reversal in buoyancy-opposed and -assisted flows are shown in Figs. 8(a) and (b), respectively. Since the effect may suppress the buoyancy effect, it is expected that the FRF region can also be expanded in both the buoyancy-assisted and buoyancy-opposed flows.

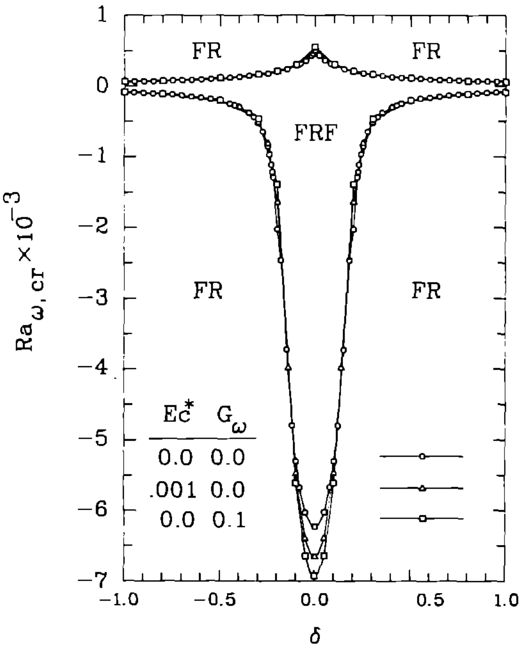

FIG. 7. Critical parameter map with stress work effects: FR, flow-reversal; FRF, flow-reversal-free.

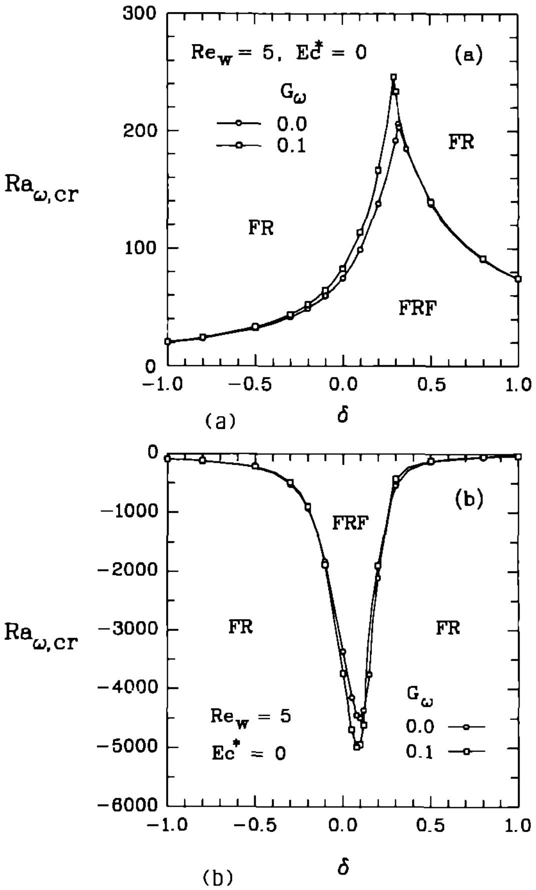

FIG. 8. Stress work effects on critical conditions of flow-reversal in a rotating semiporous-walled channel: (a) buoyancy-opposed flows; (b) buoyancy-assisted flows.

CONCLUDING REMARKS

The similarity solution has been obtained to analyze the mixed convection in radially rotating channels. In the simple theoretical model many significant results, that is, the velocity and temperature distributions, flow and heat transfer characteristics with the effects of wall-transpiration, centrifugal-buoyancy and, especially, the stress work effects are addressed. The threshold of flow-reversal in the radially rotating channels are also included. It is believed that this solution is valuable for the understanding of the non-isothermal rotating flows.

In class 2, that is, one-side porous-walled channel, the similarity model is restricted only to the cases with $Ec^* = 0$. In buoyancy-assisted flows, the stress work effects can always reduce the heat transfer; however, in buoyancy-opposed ones, the heat transfer rate may be enhanced or reduced under different conditions. Flow-reversal phenomena can be induced by the buoyancy and wall-transpiration effects. Two modes, WFR and IFR, are possible depending on the different wall-heating conditions. The stress work generates the internal heating effect and reduce the buoyancy effect. Therefore, they can delay the flow-reversal by the centrifugal-buoyancy effect. The effects are more noticeable at large Rayleigh numbers.

REFERENCES

1. Y. Mori and N. Nakayama, Convective heat transfer in rotating radial circular pipes (1st report, laminar region), *Int. J. Heat Mass Transfer* **11**, 1027–1040 (1968).
2. R. Siegel, Analysis of buoyancy effect on fully developed laminar heat transfer in a rotating tubes, *ASME Trans. J. Heat Transfer* **105**, 338–344 (1985).
3. D. Skiadaressis and D. B. Spalding, Heat transfer in a pipe rotating around a perpendicular axis, HTS/77/3, Mech. Engng Dept, Imperial College of Science and Technology, London, U.K. (1977).
4. H. Iacovides and B. E. Launder, Parametric and numerical study of fully developed flow and heat transfer in rotating rectangular ducts, *ASME Trans., J. Turbomachinery* **113**, 331–338 (1991).
5. S. P. Harasgama and W. D. Morris, The influence of rotation on the heat transfer characteristics of circular, triangular, and square sectioned coolant passages of gas turbine rotor blades, *ASME J. Turbomachinery* **110**, 44–50 (1988).
6. J. H. Wagner, B. V. Johnson and T. J. Hajek, Heat transfer in rotating passages with square smooth walls and radial outward flow, Paper No. 89-GT-272, presented at the 34th Gas Turbine and Aeroengine Congress and Exposition, Toronto, Canada (1989).
7. G. J. Hwang and C. Y. Soong, Experimental automation and heat transfer measurement on a rotating thermal system. In *Transport Phenomena in Thermal Control* (Edited by G. J. Hwang), pp. 375–388. Hemisphere, New York (1989).
8. C. Y. Soong, S. T. Lin and G. J. Hwang, An experimental study of convective heat transfer in radially rotating rectangular ducts, *ASME Trans. J. Heat Transfer* **113**, 604–611 (1991).
9. W. D. Morris and G. Ghavami-Nasr, Heat transfer measurements in rectangular channels with orthogonal mode rotation, *ASME Trans., J. Turbomachinery* **113**, 339–345 (1991).
10. S. L. Moskowitz and S. Lombardo, 2750 Deg F engine test of a transpiration air-cooled turbine, *ASME J. Engng Pwr* **93**, 238–248 (1971).
11. R. Raj, Deposition results of a transpiration air-cooled turbine vane cascade in a contaminated gas stream, *ASME Trans. J. Engng Pwr* **105**, 826–833 (1983).
12. V. M. Epifanov, A. A. Kurakin and Yu. A. Rusetskii, The effect of heat transfer to transpiration-cooled turbine blades, *Thermal Engng* **33**(8), 441–445.
13. C. Y. Soong and G. J. Hwang, Laminar mixed convection in radially rotating semiporous channels, *Int. J. Heat Mass Transfer* **33**, 1805–1816 (1990).
14. J. A. D. Ackroyd, Stress work effects in laminar flat-plate natural convection, *J. Fluid Mech.* **62**(4), 677–695 (1974).
15. D. L. Turcotte, A. T. Hsui, K. E. Torrance and G. Schubert, Influence of viscous dissipation on Benard convection, *J. Fluid Mech.* **64**(2), 369–374 (1974).
16. D. L. Turcotte, D. A. Spence and H. H. Bau, Multiple solutions for natural convective flows in an internally heated, vertical channel with viscous dissipation and pressure work, *Int. J. Heat Mass Transfer* **25**, 699–706 (1982).
17. M. Iqbal, B. D. Aggarwala and M. S. Rokerya, Viscous dissipation effects on combined free and forced convection through vertical circular tubes, *ASME Trans. J. Appl. Mech.* 931–935 (December 1970).
18. P. M. Beckett, Combined natural- and forced-con-

vection between parallel vertical walls, *SIAM J. Appl. Math.* **39**(2), 372–384 (1980).
19. P. M. Beckett and I. E. Friend, Combined natural and forced convection between parallel walls: developing flow at high Rayleigh numbers, *Int. J. Heat Mass Transfer* **27**, 611–621 (1984).
20. J. W. Chew, Effect of frictional heating and compressive work in rotating axisymmetric flow, *ASME J. Heat Transfer* **107**, 984–986 (1985).
21. W. Kuhl, Investigations on the local heat transfer coefficient of convection cooled rotor blades, *AGARD CP-229, High Temperature Problems in Gas Turbine Engines*, pp. 7-1 to 7-11 (September 1977).

APPENDIX: ANALYTIC SOLUTIONS FOR $Re_w = Ec^* = 0$

(1) $Ra_\omega = 0$ (forced convection):

$$f(y) = 3y^2 - 2y^3 \tag{A1}$$

$$g(y) = [\delta - \tfrac{1}{2}(1 - G_\omega)]y + (1 - G_\omega)(y^3 - \tfrac{1}{2}y^4). \tag{A2}$$

(2) $Ra_\omega > 0$ (buoyancy-opposed mixed convection):

$$f(y) = C_1 + C_2 \sinh Ky + C_3 \cosh Ky + C_4 \sin Ky + C_5 \cos Ky \tag{A3}$$

$$g(y) = \delta y + \frac{1}{K}(1 - G_\omega)\{C_2[(\cosh Ky + \cos Ky) - y(\cosh K + \cos K) - 2(1-y)] + C_3(\sinh Ky - y \cdot \sinh K) + C_5(\sin Ky - y \cdot \sin K)\} \tag{A4}$$

where, by defining $\delta^* = \delta/(1 - G_\omega)$

$$C_5 = \frac{1}{\Delta_1}\{2 \sinh K(1 - \cos K) - K\delta^*[\sin K \cdot \sinh K - (1 + \cos K)(\cosh K - 1)]\};$$

$$C_4 = \frac{1}{\Delta_1}\{K\delta^*[\sinh K(\cos K - 1) + \sin K(\cosh K - 1)] - 2 \sin K \sinh K\};$$

$$C_3 = C_4(\cosh K - \cos K)/\sinh K + C_5 \sin K/\sinh K;$$

$$C_2 = -C_4; \quad C_1 = -C_3 - C_5;$$

$$\Delta_1 = -4[\sinh K(1 - \cos K) - \sin K(\cosh K - 1)];$$

$$K = [Ra_\omega(1 - G_\omega)]^{1/4}.$$

(3) $Ra_\omega < 0$ (buoyancy-assisted mixed convection):

$$f(y) = \frac{f''(0)}{2a^2} \sin ay \cdot \sinh ay + \frac{f'''(0)}{4a^3}(\sin ay \cdot \cosh ay - \cos ay \cdot \sinh ay) + \frac{f^{\mathrm{iv}}(0)}{4a^4}(1 - \cos ay \cdot \cosh ay) \tag{A5}$$

$$g(y) = \delta y - \frac{f''(0)}{4a^3}[\sin ay \cdot \cosh ay - \cos ay \cdot \sinh ay - y(k_2 - k_3)] - \frac{f'''(0)}{4a^4}[1 - \cos ay \cdot \cosh ay - y(1 - k_4)] + \frac{f^{\mathrm{iv}}(0)}{8a^5}[\sin ay \cdot \cosh ay - \cos ay \cdot \sinh ay - y(k_2 + k_3)] \tag{A6}$$

where

$$f''(0) = \frac{1}{\Delta_2}[8a^6\delta^*(k_2 - k_3)^2 - 8a^5k_1(k_2 + k_3) - 8a^5(1 - k_4)(k_2 - k_3) - 16a^6\delta^*k_1(1 - k_4)];$$

$$f'''(0) = \frac{1}{\Delta_2}[8a^6(k_2 - k_3)^2 + 16a^7\delta^*(1 - k_4)(k_2 + k_3) + 8a^6(k_2 + k_3)^2 - 16a^7\delta^*k_1(k_2 - k_3)];$$

$$f^{\mathrm{iv}}(0) = \frac{1}{\Delta_2}[16a^7(1 - k_4)(k_2 + k_3) + 32a^8\delta^*k_1^2 - 16a^8\delta^*(k_2^2 - k_3^2) - 16a^7k_1(k_2 - k_3)];$$

$$\Delta_2 = 2a^3(k_2 - k_3)^3 + 4a^3(1 - k_4)^2(k_2 + k_3) - 4a^3k_1^2(k_2 + k_3) + 2a^3(k_2 + k_3)(k_2^2 - k_3^2) - 8a^3k_1(1 - k_4)(k_2 - k_3);$$

$$k_1 = \sin a \cdot \sinh a; \quad k_2 = \sin a \cdot \cosh a;$$

$$k_3 = \cos a \cdot \sinh a; \quad k_4 = \cos a \cdot \cosh a;$$

$$a = [-Ra_\omega(1 - G_\omega)/4]^{1/4}.$$